Nuclear Quantum Memory and Time Sequencing of a Single γ Photon

Xiwen Zhang, Wen-Te Liao, Alexey Kalachev, Rustem Shakhmuratov, Marlan Scully, and Olga Kocharovskaya

Phys. Rev. Lett. **123**, 250504 — Published 18 December 2019

DOI: 10.1103/PhysRevLett.123.250504

Nuclear quantum memory and time sequencing of a single γ photon

Xiwen Zhang,[1,*] Wen-Te Liao,[1,2] Alexey Kalachev,[3] Rustem Shakhmuratov,[3] Marlan Scully,[1,4] and Olga Kocharovskaya[1,†]

[1] *Department of Physics and Astronomy, Texas A&M University, College Station, Texas 77843, USA*
[2] *Department of Physics, National Central University, Taoyuan City 32001, Taiwan*
[3] *Zavoisky Physical-Technical Institute, FRC Kazan Scientific Center of RAS, Sibirsky Trakt 10/7, Kazan 420029, Russia*
[4] *Baylor University, Waco, Texas 76706, USA*

(Dated: November 26, 2019)

We propose a technique for γ photon quantum memory through a Doppler frequency comb, produced by a set of resonantly absorbing nuclear targets that move with different velocities. It provides a reliable storage, an on-demand generation, and a time sequencing of a single γ photon. This scheme presents the first γ-photon-nuclear-ensemble interface opening a new direction of research in quantum information science.

PACS numbers: 76.80.+y, 07.85.Fv, 42.50.Md, 42.50.Ex, 42.50.-p

In the last decade optical-atomic interfaces have been developed as one of the basic building blocks for quantum information processing [1]. Recent advancement in tools and techniques for the coherent control of γ rays [2–22] allows to envision a complementary quantum information platform based on γ-ray-nuclear interfaces. The main advantages of a γ photon over an optical photon lie in its almost perfect detectability and much tighter, potentially sub-angstrom, focusability. Nuclear ensembles hold important advantages over atomic ensembles in a unique combination of high nuclear density in bulk solids with narrow, lifetime-broadening Mössbauer transitions (1 Hz - 1 MHz at nuclear density $\sim 10^{23}$ cm^{-3}) even in room temperature. This may lead to the densest long-lived room-temperature quantum memories and ultra compact nanometer-scale photon processors.

Quantum memory, representing itself as a controllable delay line for a single photon, lies in the heart of quantum computation and communication devices [23, 24]. Various techniques of quantum optical memory have been developed recently [23–28]. However, a direct transfer of these techniques from optical to γ-ray range is hardly possible. Such optical techniques, as electromagnetically induced transparency [25], off-resonant Raman [26], and atomic frequency comb (AFC) [27], imply a presence of strong coherent driving fields, which are not available yet. Meanwhile, as far as a gradient echo memory (GEM) technique [28] is concerned, it would require a strong (due to the small value of nuclear magneton) and fast-switchable external magnetic field ($\sim$ 10 T switched within $\sim$ 10 ns in the case of ^{57}Fe [29]).

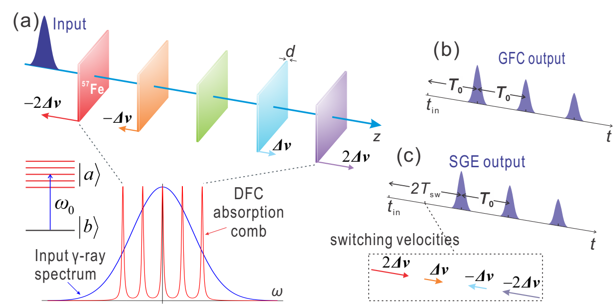

FIG. 1. (Color online) Illustration of γ-ray nuclear quantum memory. (a) The input single γ-photon wave packet is absorbed by the Doppler frequency comb, formed by a number of Mössbauer targets, moving with velocities $v_m = m\Delta v$, $m = 0, \pm1, \pm2, \cdots, \pm(M-1)/2$. (b) In GFC regime, the periodic beating between spectral components of the polarization in different targets forms the echo signal. (c) In SGE regime, the velocity directions of all targets are switched to the opposite at the moment $t_{\rm in} + T_{\rm sw}$ before the appearance of the first GFC echo. The phases of the targets' polarizations spread before switching and rewind after switching, so that an echo emerges at twice of the switching time $t_{\rm in} + 2T_{\rm sw}$.

We propose to store a single γ-ray wave packet of central frequency ω_0, full-width-half-maximum (FWHM) field duration Δt and arrival time $t_{\rm in}$ in a two-level nuclear resonant medium composed of M identical Mössbauer targets, which have the same optical thickness ζ^0 and move at different velocities v_m with equal velocity spacing Δv [Fig. 1(a)]. Due to Doppler effect, such velocity distribution forms a frequency comb in the resonant absorption spectrum of that set of targets with teeth separation $\beta\omega_0$,

* Department of Physics and Astronomy, University of Toronto, 60 Saint George Street, Toronto, Ontario M5S 1A7, Canada
† kochar@physics.tamu.edu

teeth width 2Γ (where $\beta = \Delta v/c$ and Γ is a decay rate of nuclear coherence), and corresponding finesse $\mathcal{F} = \beta\omega_0/(2\Gamma)$. We call it a Doppler frequency comb. The total spectral width of this comb $M\beta\omega_0$ is chosen to overlap the spectrum of a signal pulse to provide its resonant absorption during the storage stage which duration is limited by the collective polarization decay time T_2. A retrieval of the stored pulse can be accomplished in two different ways based on two different physical mechanisms.

First, the periodic structure of the absorbing frequency comb guarantees an automatic retrieval of single γ photon at integer multiples of the rephasing time $T_0 = 2\pi/(\beta\omega_0)$ [see Fig. 1(b)]. This regime is similar to the AFC memory used in the optical range, but the technique for the comb formation is completely different. In the optical regime it is based on optical pumping of an absolute majority of atoms within a large inhomogenously broadened profile into an auxiliary state) [27] (which implies a presence of both large inhomogenous broadening and an auxiliary level) under the action of a proper train of sufficiently strong optical pulses. This results in a relatively low contrast frequency comb with all spectral components present together in each point of the medium. In our case, a high contrast frequency comb is formed via the Doppler effect, with its spectral components distributed along the photon propagation direction. For this reason we call this regime the gradient frequency comb (GFC) memory.

The presence of the frequency gradient along the photon propagation path allows the realization of the second type of the readout technique, namely, via simultaneous reversing of all the targets' velocities ($v_m \to -v_m$) at some moment of time $t_{\rm in} + T_{\rm sw}$, before the appearance of the first GFC echo [see Fig. 1(c)]. Such a switch enforces a rewind of the phase evolution of the polarizations in the moving targets. The echo is formed when the phases of polarizations regress back to their original state, resulting in a constructive interference. This regime is similar to GEM in the optical range, but its mechanism of the frequency gradient formation is different. In the optical range it is formed via dc Stark or Zeeman effect by an application of a nonuniform electric or magnetic field with a longitudinal gradient [28] (which implies a presence of a sufficiently large difference between dipole moments of the ground and excited states). In our case, the frequency gradient is induced by the motion of the targets with different velocities via the Doppler effect, resulting in a stepwise frequency change (instead of a continuous change in the traditional optical schemes). For this reason we call this regime the stepwise gradient echo (SGE) memory.

Let the $m^{\rm th}$ Mössbauer target have the initial central position l_m, thickness d, nuclear density N, and resonant frequency detuning $\Delta_m = m\beta\omega_0$. The light-matter interaction in a one-dimensional model is described by the Maxwell-Bloch equations (see Supplemental Material for details):

$$\frac{\partial}{\partial z}\mathcal{E}(z,t) = \sum_{m=-M_0}^{M_0} \mathcal{P}^m(z,t)\left(\Theta_-^m - \Theta_+^m\right), \tag{1}$$

$$\frac{\partial}{\partial t}\mathcal{P}^m(z,t) = (-\Gamma - i\Delta_m)\mathcal{P}^m(z,t) - |g|^2 N\mathcal{E}(z,t), \tag{2}$$

where $\mathcal{E}$ is the slowly varying amplitude of the γ-ray field, $\mathcal{P}^m$ is proportional to the slowly varying amplitude of the off-diagonal element of the density matrix for the $m^{\rm th}$ target, g is the coupling constant of the γ ray-nucleus interaction, $\zeta^0 = 2|g|^2 Nd/\Gamma$, and $\Theta_\pm^m = \Theta(z - l_m \mp d/2)$ is the Heaviside step function.

As an example, we consider an input single photon of duration $\Delta t = 7$ ns with central frequency on resonance with the 14.4 keV nuclear transition of ^{57}Fe [16, 17]. The resonant medium consists of five ^{57}Fe-enriched stainless-steel foils, each with $\zeta^0 = 41.3$ (corresponding to a total optical thickness $\zeta = M\zeta^0 = 206.5$) and $\Delta v = 3.075$ mm/s [30, 31]. As shown in Fig. 2(a), the photon is automatically retrieved via the GFC mechanism with an efficiency $\approx 45\%$ after being stored for 28 ns [see Eqs. (S18) and (S19) in the Supplemental Material for the definition of efficiency η and fidelity $\mathscr{F}$].

Unless otherwise specified, we mainly focus on the first echo pulse. In GFC regime, this is obtained by solving Eqs. (1) and (2) [32, 33]:

$$\mathcal{E}_{\rm out}(t) \approx e^{-\frac{\pi}{4}\zeta^0_{\rm eff}}\mathcal{E}_{\rm in}(t) - \frac{\pi\zeta^0_{\rm eff}}{2}e^{-\frac{\pi\zeta^0_{\rm eff}}{4}}e^{-\frac{\pi}{\mathcal{F}}}\mathcal{E}_{\rm in}(t - T_0), \tag{3}$$

where $\zeta^0_{\rm eff} = \zeta^0/\mathcal{F}$ is an individual effective optical thickness. The first term of Eq. (3) is the leakage field, i.e. the field not absorbed by the comb, and the second term represents the first GFC echo pulse.

According to Eq. (3), the first GFC echo efficiency is $\eta_{\rm G1} = \left(\frac{\pi\zeta^0_{\rm eff}}{2}e^{-\frac{\pi\zeta^0_{\rm eff}}{4}}e^{-\frac{\pi}{\mathcal{F}}}\right)^2$. Its upper bound 54% can be achieved by optimizing the optical thickness and the finesse at the following conditions [35]:

$$\zeta^0 \approx \frac{4}{\pi}\mathcal{F} \gg 1, \tag{4}$$

$$\frac{\pi}{M\Delta t\Gamma} < \mathcal{F} < \frac{\pi}{\Delta t\Gamma}. \tag{5}$$

From Eq. (4), in order to reduce the role of decoherence, a high finesse is required. But at high finesse the portion of the full comb bandwidth covered by the comb teeth is too small to retain the input energy. To achieve the optimal storage efficiency, one has to effectively broaden each comb tooth by means of optical thickness such that $\zeta^0 2\Gamma \approx \beta\omega_0$ in accordance with Eq. (4). Additional condition (5) is required to ensure spectrum coverage and echo's temporal resolvability, which is clear after being unfolded into $1/M < \beta\omega_0/(2\pi/\Delta t) < 1$ or $\Delta t < T_0 < M\Delta t$. The GFC regime can also be used as a way to split a single-peak γ photon into a time-bin waveform. An equal splitting of an input photon between the leaked and delayed fractions of the output photon is achieved at the optical thickness $\zeta^0_{\rm eff} = (2/\pi)e^{\pi/\mathcal{F}}$, with conversion efficiency 50% for $\mathcal{F} = 10$.

Essentially higher efficiency than the upper bound of GFC echo 54% can be achieved using SGE mechanism implemented by switching the directions of motion of all targets to the opposite at $t_{\rm in} + T_{\rm sw}$ [Fig. 1(c)]. The switch time is chosen to satisfy $\Delta t/2 < T_{\rm sw} < T_0 - \Delta t/2$, so that the SGE echo appears as the first retrieval signal (see Fig. 3) [38]. Thus the storage time of the signal, $2T_{\rm sw}$, can be completely controlled over the time interval $(\Delta t, 2T_0 - \Delta t)$, allowing to produce a γ photon on demand.

The SGE echo efficiency is on the order of $\sim \left(1 - e^{-\pi\zeta^0_{\rm eff}/2}\right)^2 e^{-4\Gamma T_{\rm sw}}$ by assuming the ratio of the retrieved over the stored energy is the same as the ratio of the stored over the input energy. In the limit of large number of targets ($M \to \infty$) SGE regime transforms into GEM scheme, which may provide 100% efficiency when the decoherence effects are small enough [42]. Hence simply by splitting the same total optical thickness into more targets, we can increase the storage efficiency and, in particular, make it higher than the theoretical upper limit of the efficiency in the GFC regime [see Fig. 3(a)]. Specifically, the storage of a 7 ns photon for 42 ns in ^{57}Fe with total optical thickness 206.7 demonstrates an efficiency of 57.9% by using $M = 31$ discrete Mössbauer targets in SGE regime, close to the $\sim 63\%$ efficiency of the continuous limit.

The Doppler frequency comb allows one to realize not only storage, but also a variety of single-photon processing functionalities, including reversing of the photon's temporal shape, delayed and/or advanced retrieval, relative amplitude manipulation, temporal permutation, etc., which can be achieved by a modulation of the targets' velocities before the emergence of the echo. For example, by choosing either GEM or SGE regime one can retrieve a time-bin qubit in the same or reversed order of the input signal [Figs. 4(a-b)]. By stopping all targets after absorption, one can hold the echo for an arbitrary time [Figs. 4(c-d)]. By boosting all targets' velocities via increasing velocity spacing Δv to $\Delta v'$ and back to Δv in a time interval $t \in (t'_i, t'_f)$, one can impose additional phase difference $\Delta\phi = (\Delta v' - \Delta v)\omega_0(t'_f - t'_i)/c \in [0, 2\pi]$ between polarizations of two adjacent targets. Consequently, the first echo right after modulation will emerge at shifted moment of time $t_{\rm in} + \left(p - \frac{\Delta\phi}{2\pi}\right)T_0$, where $p = \left\lceil \frac{t'_f - t_{\rm in}}{T_0} + \frac{\Delta\phi}{2\pi} \right\rceil$, and $\lceil x \rceil$ represents the smallest integer greater than or equal to x. In this way it becomes possible to manipulate the time of appearance of any individual peak from the incoming photon's waveform. For such processing, only the total phase difference matters, so that the modulation does not need to be square-shape [Figs. 4(e-f)].

The presence of incoherent decay strongly limits the efficiency of all quantum memory and processing schemes. In our case, higher efficiency can be achieved for the storage of a shorter photon in a smaller interval of time during which the incoherent decay remains negligible. On the other hand, longer photons with duration over a few nanoseconds can be efficiently stored in targets with longer lived Mössbauer nuclear transitions, such as 93.3 keV transition in ^{67}Zn with coherence time 13.6 μs [43]. There are also Mössbauer transitions with lifetimes much longer than tens of microseconds, such as 12.4 keV transition in ^{45}Sc with lifetime 0.46 s, and 88.0 keV transition in ^{109}Ag with lifetime 57.1 s [43]. These transitions may be inhomogeneously broadened due to magnetic dipole-dipole interactions [44]. Potentially, these interactions may be suppressed using techniques similar to those developed in nuclear magnetic resonance (see Ref. [45] and references therein), providing extraordinarily long storage time.

We gratefully acknowledge the support by the National Science Foundation (Grant No. PHY-150-64-67 and PHY-182-09-30), as well as by AFOSR (Grant No. FA9550-18-1-0141) and ONR (Grant No. N00014-16-1-3054). X.Z. acknowledges the support by the Herman F. Heep and Minnie Belle Heep Texas A&M University Endowed Fund held/administered by the Texas A&M Foundation. W.L. is supported by the Ministry of Science and Technology, Taiwan (Grant No. MOST107-2112-M-008-007-MY3 and Grant No. MOST 107-2745-M-007-001-) and the National Center for Theoretical Sciences, Taiwan. A.K. acknowledges the financial support from the Government of the Russian Federation (Mega-Grant No. 14.W03.31.0028). R.S. acknowledges the support from the Program of Competitive Growth of Kazan Federal University funded by the Russian Government. A.K. and R.S. acknowledge the financial support from the government assignment for FRC Kazan Scientific Center of RAS.

[1] K. Hammerer, A. S. Sørensen, and E. S. Polzik, Reviews of Modern Physics **82**, 1041 (2010).
[2] P. Helistö, I. Tittonen, M. Lippmaa, and T. Katila, Physical Review Letters **66**, 2037 (1991).
[3] Y. V. Shvyd'ko, S. L. Popov, and G. V. Smirnov, Journal of Physics-Condensed Matter **5**, 1557 (1993).
[4] Y. V. Shvyd'ko, T. Hertrich, J. Metge, O. Leupold, E. Gerdau, and H. D. Rüter, Physical Review B **52**, R711 (1995).
[5] Y. V. Shvyd'ko, T. Hertrich, U. van Bürck, E. Gerdau, O. Leupold, J. Metge, H. D. Rüter, S. Schwendy, G. V. Smirnov, W. Potzel, and P. Schindelmann, Physical Review Letters **77**, 3232 (1996).
[6] R. Coussement, Y. Rostovtsev, J. Odeurs, G. Neyens, H. Muramatsu, S. Gheysen, R. Callens, K. Vyvey, G. Kozyreff, P. Mandel, R. Shakhmuratov, and O. Kocharovskaya, Physical Review Letters **89**, 107601 (2002).
[7] A. Pálffy, C. H. Keitel, and J. Evers, Physical Review Letters **103**, 017401 (2009).
[8] Y. Shvyd'ko, S. Stoupin, V. Blank, and S. Terentyev, Nature Photonics **5**, 539 (2011).
[9] J. Amann, W. Berg, V. Blank, F. J. Decker, Y. Ding, P. Emma, Y. Feng, J. Frisch, D. Fritz, J. Hastings, Z. Huang, J. Krzywinski, R. Lindberg, H. Loos, A. Lutman, H. D. Nuhn, D. Ratner, J. Rzepiela, D. Shu, Y. Shvyd'ko, S. Spampinati, S. Stoupin, S. Terentyev, E. Trakhtenberg, D. Walz, J. Welch, J. Wu, A. Zholents, and D. Zhu, Nature Photonics **6**, 693 (2012).
[10] R. Röhlsberger, H. C. Wille, K. Schlage, and B. Sahoo, Nature **482**, 199 (2012).
[11] S. Shwartz, R. N. Coffee, J. M. Feldkamp, Y. Feng, J. B. Hastings, G. Y. Yin, and S. E. Harris, Physical Review Letters **109**, 013602 (2012).
[12] X. Zhang and A. A. Svidzinsky, Physical Review A **88**, 033854 (2013).
[13] B. W. Adams, C. Buth, S. M. Cavaletto, J. Evers, Z. Harman, C. H. Keitel, A. Pálffy, A. Picon, R. Röhlsberger, Y. Rostovtsev, and K. Tamasaku, Journal of Modern Optics **60**, 2 (2013).
[14] K. P. Heeg, H. C. Wille, K. Schlage, T. Guryeva, D. Schumacher, I. Uschmann, K. S. Schulze, B. Marx, T. Kämpfer, G. G. Paulus, R. Röhlsberger, and J. Evers, Physical Review Letters **111**, 073601 (2013).
[15] T. Osaka, M. Yabashi, Y. Sano, K. Tono, Y. Inubushi, T. Sato, S. Matsuyama, T. Ishikawa, and K. Yamauchi, Optics Express **21**, 2823 (2013).
[16] F. Vagizov, V. Antonov, Y. V. Radeonychev, R. N. Shakhmuratov, and O. Kocharovskaya, Nature **508**, 80 (2014).
[17] R. N. Shakhmuratov, F. G. Vagizov, V. A. Antonov, Y. V. Radeonychev, M. O. Scully, and O. Kocharovskaya, Physical Review A **92**, 023836 (2015).
[18] K. P. Heeg, J. Haber, D. Schumacher, L. Bocklage, H.-C. Wille, K. S. Schulze, R. Loetzsch, I. Uschmann, G. G. Paulus, R. Rüffer, R. Röhlsberger, and J. Evers, Physical Review Letters **114**, 203601 (2015).
[19] W.-T. Liao and S. Ahrens, Nature Photonics **9**, 169 (2015).
[20] K. P. Heeg, A. Kaldun, C. Strohm, P. Reiser, C. Ott, R. Subramanian, D. Lentrodt, J. Haber, H. C. Wille, S. Goerttler, R. Rüffer, C. H. Keitel, R. Röhlsberger, T. Pfeifer, and J. Evers, Science **357**, 375 (2017).
[21] G.-Y. Wang and W.-T. Liao, Physical Review Applied **10**, 014003 (2018).
[22] S. Goerttler, K. Heeg, A. Kaldun, P. Reiser, C. Strohm, J. Haber, C. Ott, R. Subramanian, R. Röhlsberger, J. Evers, and T. Pfeifer, Physical Review Letters **123**, 153902 (2019).
[23] A. I. Lvovsky, B. C. Sanders, and W. Tittel, Nature Photonics **3**, 706 (2009).
[24] M. Afzelius, N. Gisin, and H. de Riedmatten, Physics Today **68**, 42 (2015).
[25] T. Chanelière, D. N. Matsukevich, S. D. Jenkins, S.-Y. Lan, T. A. B. Kennedy, and A. Kuzmich, Nature **438**, 833 (2005).
[26] K. F. Reim, P. Michelberger, K. C. Lee, J. Nunn, N. K. Langford, and I. A. Walmsley, Physical Review Letters **107**, 053603 (2011).
[27] M. Afzelius, C. Simon, H. de Riedmatten, and N. Gisin, Physical Review A **79**, 052329 (2009).
[28] G. Hétet, J. J. Longdell, M. J. Sellars, P. K. Lam, and B. C. Buchler, Physical Review Letters **101**, 203601 (2008).
[29] B. W. Adams, Journal of Modern Optics **58**, 1638 (2011).
[30] T. E. Cranshaw and J. P. Schiffer, Proceedings of the Physical Society **84**, 245 (1964).
[31] N. N. Greenwood and T. C. Gibb, Mössbauer spectroscopy (Chapman and Hall Ltd, London, 1971).
[32] X. Zhang, arXiv:1602.05115.
[33] See Supplemental Material for more information, which includes Ref. [34].
[34] T. Chanelière, J. Ruggiero, M. Bonarota, M. Afzelius, and J.-L. L. Gouët, New Journal of Physics **12**, 023025 (2010).
[35] See Supplemental Material for more discussion, which includes Refs. [36,37].
[36] X. Zhang, A. Kalachev, and O. Kocharovskaya, Physical Review A **87**, 013811 (2013).
[37] X. Zhang, A. Kalachev, and O. Kocharovskaya, Physical Review A **90**, 052322 (2014).
[38] See Supplemental Material for the feasibility of the experimental demonstration, which includes Refs. [39-41].
[39] I. Tittonen, M. Lippmaa, P. Helistö, and T. Katila, Physical Review B **47**, 7840 (1993).
[40] R. N. Shakhmuratov, F. Vagizov, and O. Kocharovskaya, Physical Review A **84**, 043820 (2011).

[41] R. N. Shakhmuratov, F. Vagizov, and O. Kocharovskaya, Physical Review A **87**, 013807 (2013).
[42] S. A. Moiseev and N. M. Arslanov, Physical Review A **78**, 023803 (2008).
[43] Y. V. Shvyd'ko and G. V. Smirnov, Nucl. Instrum. Methods Phys. Res. B **51**, 452 (1990).
[44] P. Boolchand, Journal of Quantitative Spectroscopy & Radiative Transfer **40**, 777 (1988).
[45] P. Anisimov, Y. Rostovtsev, and O. Kocharovskaya, Physical Review B **76**, 094422 (2007).

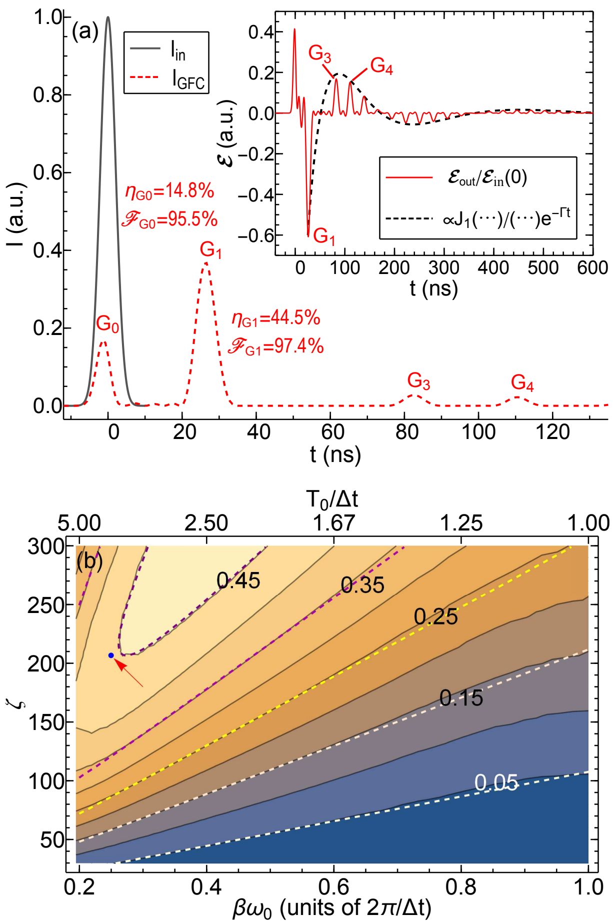

FIG. 2. (Color online) Gradient frequency comb (GFC) memory. (a) Input ($I_{\rm in}$) and output ($I_{\rm GFC}$) intensities as functions of time from numerical simulation of Eqs. (1) and (2). The input field has FWHM duration $\Delta t = 7$ ns (intensity FWHM 4.95 ns). The medium is composed of $M = 5$ ^{57}Fe-enriched Mössbauer targets with $\Gamma/(2\pi) = 0.55$ MHz, $\mathcal{F} = 32.47$ and $\zeta^0_{\rm eff} = 1.27$. The peaks $G_{1,3,4}$ are GFC echoes ($T_0 = 28$ ns). The inset shows higher sequence of GFC echoes described by the response function $\propto e^{-\Gamma t} J_1(2\sqrt{\zeta^0\Gamma t/2})/\sqrt{\zeta^0\Gamma t/2}$ [see Eq. (S45) in Supplemental Material]. (b) Numerical simulation (background contour plot) and analytical calculation [based on Eq. (3)] (dashed lines) of the GFC echo efficiency as a function of the total optical thickness $\zeta = M\zeta^0$ and the frequency comb spacing $\beta\omega_0$ for the same parameters (M, Δt, Γ) as in (a), satisfying the constrain given by Eq. (5). Graph (a) is plotted for the parameters corresponding to the point indicated by the arrow.

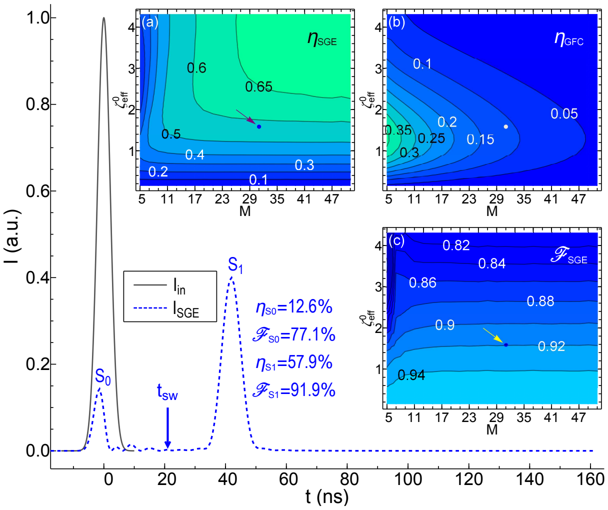

FIG. 3. (Color online) Stepwise gradient echo (SGE) memory. Input ($I_{\rm in}$) and output ($I_{\rm SGE}$) γ photon intensities as functions of time for $M = 31$ targets, each with an optical thickness $\zeta^0 = 206.7/31 = 6.67$. Inset (a) is the numerical simulation of SGE first echo efficiencies as functions of individual effective optical thickness $\zeta^0_{\rm eff}$ and number of targets M. For comparison, the color map of GFC first echo efficiencies is given in Inset (b) for the same set of parameters except there is no switching of the velocities of the targets. Inset (c) shows the numerical simulation of SGE first echo fidelity $\mathscr{F}$ as a function of $\zeta^0_{\rm eff}$ and M. All figures are plotted for the input pulse duration $\Delta t = 7$ ns and fixed comb bandwidth $M\beta\omega_0 = 2\pi/\Delta t$. The switching time in the main plot and (a, b) is $T_{\rm sw} = 21$ ns. The arrows in the insets indicate the parameters corresponding to the main plot.

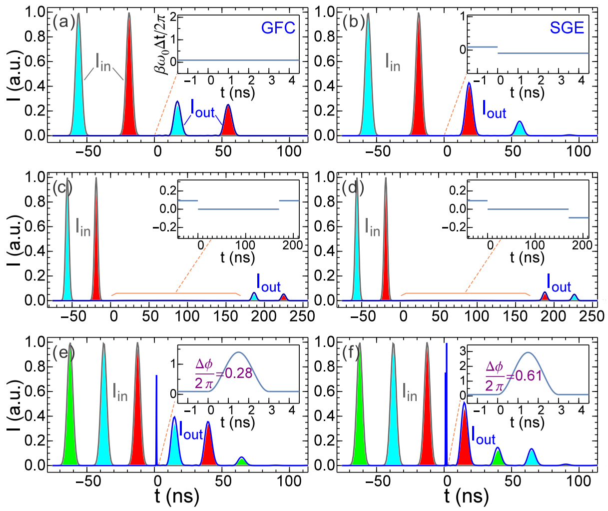

FIG. 4. (Color online) Single γ photon processing. The multi-peak input and output signals as functions of time (leakage at $t < 0$ ns is not plotted). The filled colors correspond to single-peak input (output) signals. The insets show the velocity modulation. The common parameters are: $\Delta t = 7$ ns, $T_0 = 75$ ns, $\zeta^0 = 15.4$ and $M = 13$. (a, b) GFC and SGE echoes. (c, d) Holding a double-peak signal by stopping all targets for 170 ns (i.e. longer than excited state lifetime, 141 ns) and retrieving it in the same (c) and reversed (d) order. (e, f) Circular permutations of the input triple-peak signal via sinusoidal modulation of the velocities that produces an additional phase difference $\Delta\phi/(2\pi)$ equal to 0.28 (e) and 0.61 (f). The narrow peaks in the vicinity of $t = 0$ are the losses during the modulations.